Available online at www.sciencedirect.com
SCIENCE DIRECT®
Journal of Sound and Vibration 275 (2004) 515–532
JOURNAL OF SOUND AND VIBRATION
www.elsevier.com/locate/jsvi

Simulation of dynamic train–track interaction with state-dependent track properties

J.C.O. Nielsen*, J. Oscarsson

CHARMEC, Department of Applied Mechanics, Chalmers University of Technology, SE-412 96 Gothenburg, Sweden

Received 11 October 2002; accepted 24 June 2003

Abstract

A previously published numerical method for simulation of vertical dynamic interaction between a train and a railway track is expanded to account for state-dependent track properties. Track properties are separated into linear contributions corresponding to an unloaded track, and non-linear contributions that are dependent on the time-variant state of the different track components due to the dynamic loading from a moving train model. A complex modal superposition is adopted to decouple the equations of motion of the linear track model with a non-proportional spatial distribution of viscous damping. The state-dependent properties are accounted for by applying equivalent transient external forces to the corresponding nodes of the linear finite element model of the track. Simulations are carried out in the time domain with a moving mass model. The need for a state-dependent track model is discussed with respect to reported field and laboratory measurements. The numerical method and the state-dependent track model are validated versus field measurements of wheel–rail contact force and rail bending moment as caused by a 100 mm long and 0.9 mm deep wheel flat.

1. Introduction

The main objective of train–track interaction modelling is to combine the components of the compound structure so that their complex dynamic interaction is represented properly. This calls for detailed mathematical models of train and track when train–track interaction is simulated in a wide frequency range. With the model presented here, the influence of load parameters such as train speed, axle load, axle base distance, rail corrugations and wheel flats on the response of various track components can be investigated. This information can be used for evaluation of the technical and economical feasibility of proposed track designs and for planning of maintenance procedures.

*Corresponding author. Tel.: +46-31-772-1500; fax: +46-31-772-3827.
E-mail address: jens.nielsen@me.chalmers.se (J.C.O. Nielsen).

0022-460X/$ - see front matter © 2003 Elsevier Ltd. All rights reserved.
doi:10.1016/j.jsv.2003.06.033

Several train and track models of different detail for simulation of train–track interaction have been proposed by various researchers, see for example the literature surveys by Knothe and Grassie [1] and Popp et al. [2]. Most of these models are linear except for the conditions at the wheel–rail contact. Not much effort has been spent on establishing mathematical models that account for the state-dependent (non-linear) behaviour of rail pads and ballast/subgrade.

Dynamic train–track interaction is studied either in the frequency domain or in the time domain. When the interaction is studied in the frequency domain, the included models must be linear. However, computing times are short compared to the time-domain methods. Another advantage is that the frequency dependence of for example rail pad and ballast/subgrade properties can readily be considered. A moving irregularity model is used. This means that the vehicle model remains in a fixed position on the rail, and an imaginary strip containing the wheel/rail irregularities is pulled at a steady speed between the models of vehicle and track [1]. The models developed by Thompson [3] and Hempelmann [4] are examples in this model category. Time-domain models, on the other hand, may account for state-dependent and randomized track properties and non-linear rolling contact mechanics. A moving mass model is adopted, where the vehicle model is moving along the track model considering the spatially varying track properties that for example occur due to the discrete sleeper supports. Examples in this category are the models developed by Nielsen et al. [5,6] and Ripke [7].

The objective of the present study is to expand a previously published model for simulation of vertical train–track interaction [5,6] to account for the state-dependent (non-linear) properties of rail pads and ballast/subgrade. In the previous model, a lumped parameter train model is moving along a linear finite element model of the track. The wheel–rail contact model is non-linear allowing for loss-of-contact and recovered contact. The train and track models are coupled through algebraic constraint equations accounting for a given train speed and given irregularities on the wheel tread and railhead. The need for a state-dependent track model will be discussed with respect to laboratory and field measurements. The numerical method and the state-dependent track model will be validated versus field measurements of wheel–rail contact force and rail bending moment as caused by a 100 mm long and 0.9 mm deep wheel flat at different train speeds. Simulation results from the state-dependent track model will be compared to those obtained when using a linear track model.

2. State-dependent track properties

Extensive field and laboratory measurements have been performed on Swedish railway tracks and on the rail pad currently used in modern Swedish tracks. In this section, some of these measurements are described along with a short discussion on the detected non-linear characteristics of certain track properties.

2.1. Field measurements of ballast/subgrade properties

Field measurements on Swedish railway tracks have been performed at several occasions by the Swedish National Rail Administration (Banverket). Modern ballasted Swedish tracks consist of concrete sleepers, UIC60 rails and Pandrol fastenings with 10 mm thick studded rubber rail pads.

The ballast, on the test site investigated here, is a 300 mm thick layer of 32–64 mm granite macadam. An instrumented stationary railway wagon (track loading vehicle (TLV)) with two vertical servo-hydraulic cylinders was used to apply loads acting either on the rails or on sleepers unfastened from the rails. The cylinders can be used for dynamic excitation with a force amplitude 5 kN up to 200 Hz. At the same time, static preloads of maximum 150 kN can be applied by each cylinder. The wagon also has a horizontal servo-hydraulic cylinder that can be used for lateral excitation. The TLV can thus provide a good description of the track dynamics in the frequency range 0–200 Hz, taking into account the influence of a high static preload representing the static wheel load. To determine the response function for the track at higher frequencies and without any static preload, the track was loaded using impulse excitation with a sledgehammer. Results from measurements performed in 1993 and 1995 by Banverket in collaboration with CHARMEC are reported by Fermér and Nielsen [8] and by Igeland and Oscarsson [9], respectively.

Track receptances measured on the rail directly above a sleeper for two different static preloads were illustrated in Ref. [9]. A strong dependence of preload was observed. In the same reference, static load–deflection characteristics measured for three adjacent sleepers that had been unfastened from the rails were reported. It was observed that the displacement of a sleeper end due to a given load magnitude varied significantly from one sleeper to the next. Although the nominal sleeper spacing was only 0.65 m, the displacements of adjacent sleeper ends due to a static 50 kN load differed by a factor of two. It was concluded that the load–deflection characteristics of the ballast/subgrade are highly non-linear. One important contribution to the non-linear behaviour was that parts of some sleeper base areas were not in contact with the ballast for the unloaded track. Instead, some sleepers primarily hung from the rails.

In the measurements reported here, the vertical cylinders on the TLV were used to apply loads on different sleepers. The measurements were performed in 2000 on the main line "Svealandsbanan" between Eskilstuna and Södertälje. This track is normally used for X2000 high-speed passenger traffic and for freight trains. The total load was applied symmetrically at positions close to the two rail seats of one sleeper for measurement of ballast/subgrade properties. Before the static and dynamic loads were applied on one sleeper, the rails were unfastened from that sleeper and the adjacent sleepers by removing the fastening clips. The load was applied at constant frequency 2 Hz, but the dynamic load amplitude was varied between different tests. The secant stiffness of the ballast/subgrade was evaluated as the range of total sleeper load during one excitation cycle over the corresponding range of sleeper displacement. In Fig. 1, the influence of maximum sleeper load on ballast/subgrade secant stiffness measured for 20 adjacent (unfastened) sleepers is illustrated. Again, a large scatter in the results is observed. Note that the relationship between secant stiffness and load is approximately linear. This indicates a non-linear load–displacement behaviour of the ballast/subgrade.

A simple estimation of loss factors for the ballast/subgrade has been performed for three adjacent sleepers. The energy dissipation (area of the hysteresis loop) E_m during one excitation cycle was estimated from the measured load–displacement characteristics for the sleeper–ballast/subgrade system. For a linear system described by a structural (hysteretic) damper with loss factor η in parallel with a linear spring with stiffness k, the hysteresis loop is elliptical and the energy dissipation E_c is determined by

$$E_c = \pi \eta k x_{max}^2. \tag{1}$$

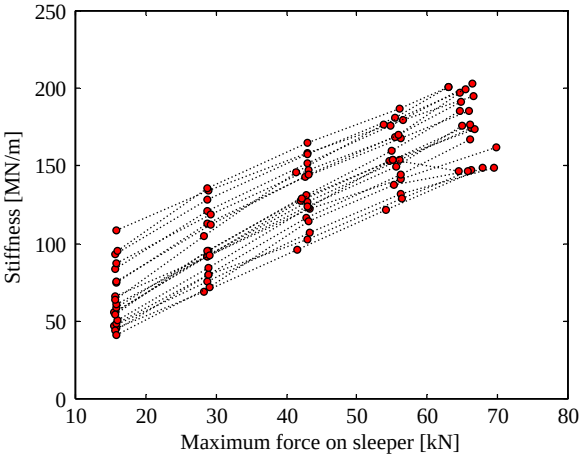

Fig. 1. Secant stiffness of ballast/subgrade versus maximum symmetric sleeper load at 2 Hz. Stiffnesses evaluated from measurements on 20 adjacent sleepers unfastened from the rails (Svealandsbanan, 2000).

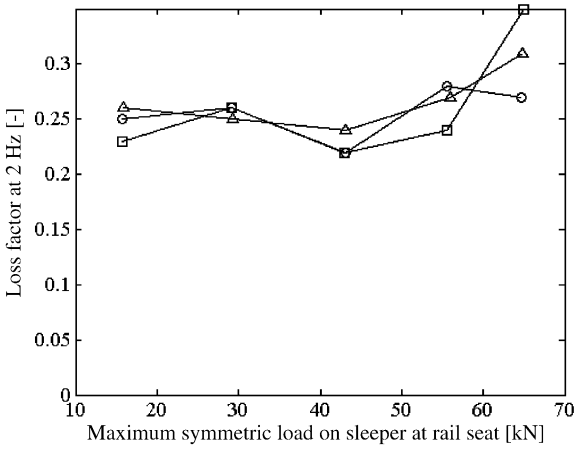

Fig. 2. Ballast/subgrade loss factor (equivalent structural damping) versus maximum symmetric sleeper load at 2 Hz. Loss factors determined for three adjacent sleepers unfastened from the rails (Svealandsbanan, 2000): –□–, sleeper 1; –○–, sleeper 2; –△–, sleeper 3.

Here x_{max} is the maximum displacement of the system when excited by a harmonic force [10]. By setting $E_c = E_m$ and adopting the secant stiffness and the maximum displacement from the measured load–displacement characteristics, the loss factor of the ballast/subgrade was determined for different maximum loads applied on the sleeper. The results shown in Fig. 2 indicate that the loss factor at 2 Hz is relatively independent of the maximum load applied on the sleeper for loads up to 2×50 kN. Unfortunately, data were only available at the frequency 2 Hz.

2.2. Laboratory measurements of rail pad properties

Stiffness and damping of the 10 mm studded rubber rail pad that is used in Sweden in modern tracks have been measured in the laboratory by Thompson and van Vliet [11]. A schematic illustration of the static and dynamic load–deformation characteristics is shown in Fig. 3(a). The rail pad was first preloaded by a given static force, which is illustrated by the dashed line. Then a cyclic loading with respect to the static equilibrium was applied. The solid arrows in Fig. 3(a) indicate the dynamic stiffness for different static preloads. For given preloads, the ratio of dynamic stiffness to static stiffness was approximately 4:1. A weak frequency dependence of dynamic rail pad stiffness and loss factor was observed. Thompson et al. [12] investigated the influence of the non-linear stiffness behaviour of rail pads on the track component of rolling noise. They concluded that neglecting the preloading effect on rail pad stiffness will lead to a significant over-prediction of the track noise.

Andersson and Oscarsson [13] adopted a state-dependent viscoelastic three-parameter model to represent the measured properties of the studded rubber rail pad (see Fig. 3(b)). Using this model, it was found that both low- and high-frequency rail pad behaviour were modelled with high accuracy. Measured data were taken from Ref. [11]. The linear rail pad properties were estimated from low-amplitude dynamics experiments on a rail pad statically preloaded with 20 kN, corresponding to the load applied by the rail fastenings. The state-dependent rail pad properties were determined through interpolation of data from low-amplitude dynamics experiments performed at five different static preload levels (20, 30, 40, 60 and 80 kN). In a demonstration example, it was however shown that the influence of the state-dependent properties of the investigated rail pad on simulated wheel–rail contact force was rather small. The calculated range of rail pad deformation during a wheel passage was in this case so limited that a linear rail pad model was sufficient.

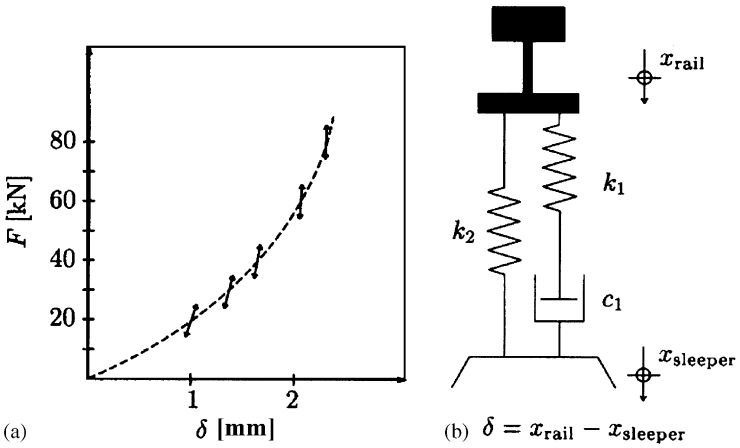

Fig. 3. (a) Schematic illustration of static and dynamic load–deflection characteristics for a 10 mm studded rubber rail pad. The rail pad was first preloaded by a given static force, which is illustrated by the dashed line. Then a cyclic loading with respect to the static equilibrium was applied. The solid arrows indicate the dynamic stiffness for the different static preloads. (b) Illustration of rail pad modelled by a viscoelastic three-parameter model. From Ref. [13].

3. State-dependent track model

Receptances measured on a railway track will be strongly dependent of the magnitude of the applied static preload. The load dependence stems primarily from the properties of rail pads and ballast/subgrade as was discussed in the previous section. These circumstances call for the use of a state-dependent track model.

The track model used here is a finite element model with state-dependent track component properties (see Fig. 4). The track and its loading are assumed to be symmetric with respect to a centreline between the two rails. Therefore, only half the track is modelled to shorten computing times. In the demonstration example presented in the following section, the length of the track model is 50 sleeper bays with clamped boundary conditions of the rail at its two ends (see Fig. 4). For the present application, the chosen number of sleeper bays is sufficient to reach a condition at the centre portion of the model where the effects from the boundaries are negligible. In each sleeper bay, the rail is described by eight Rayleigh–Timoshenko beam finite elements. The rail is discretely supported, via rail pads, by equidistant sleepers. The (half) sleepers are modelled as rigid masses. The dampings of rail pads and ballast/subgrade are modelled as being viscous in order to obtain a causal response in the time domain. In Fig. 4, the state-dependent stiffness and damping of rail pads and ballast/subgrade are denoted by k_p, c_p, k_b and c_b, respectively. Input data to the track model are listed in Table 1. Randomized track properties and sleepers modelled by Rayleigh–Timoshenko beam finite elements can be accounted for in the model, but these features are not adopted in the present study.

The stiffness and damping of rail pads and ballast/subgrade are separated in linear contributions corresponding to an unloaded track, and increments that are determined by the time-variant state of the components due to the current positions of adjacent wheel loads. To save computing times in the simulation of train–track interaction, a complex modal superposition is adopted to decouple the equations of motion for the track model with only the linear contributions and a non-proportional spatial distribution of viscous damping [6,14].

The state-dependent increments of stiffness and damping are accounted for by applying equivalent external forces to the corresponding nodes of rail and sleepers (see again Fig. 4). For

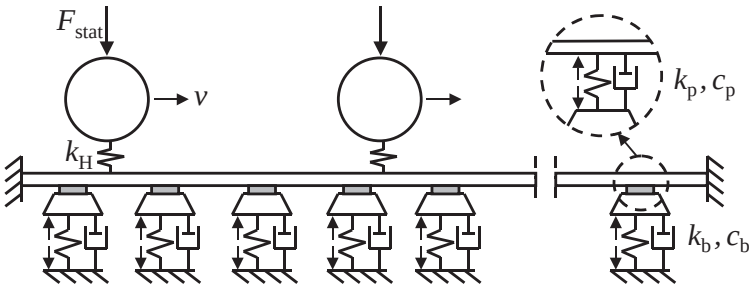

Fig. 4. Schematic illustration of the state-dependent track model used for simulation of vertical dynamic train–track interaction. Arrows in the track model indicate external transient forces acting between sleepers and rail and between sleepers and ballast/subgrade. The magnitudes of these forces are governed by the time-variant states of rail pads and ballast/subgrade.

Table 1
Summary of track and train properties

	Parameter	Value
Track component		
UIC60 rail	Bending stiffness	6.4 MN m^2
	Shear stiffness	250 MN
	Mass per unit length	60.0 kg/m
	Rotational inertia per unit length	0.24 kg m
Rail pad	Linear stiffness	80 MN/m
	Linear viscous damping	15 kNs/m
	Side length	0.15 m
Sleeper	Mass (half-sleeper)	125 kg
	Sleeper distance	0.65 m
Ballast properties per rail seat	Linear stiffness	30 MN/m
	Linear viscous damping	31 kNs/m
Train model		
	Unsprung wheelset mass	1185 kg
	Axle load	24 tonnes
	Bogie axle base	1.8 m
	Wheel diameter	900 mm
Wheel flat		
	Length	100 mm
	Depth	0.90 mm

each rail pad, the magnitude of two equal but counter-acting forces is governed by its calculated compression and compression rate. For each spring–damper system modelling the ballast/subgrade under each sleeper, the magnitude of two counter-acting forces (one force is acting on the assumingly rigid foundation under the ballast/subgrade) is determined by the calculated vertical displacement and velocity of the sleeper. In the time-stepping integration scheme, the states of rail pads and ballast/subgrade are calculated in each time-step and the forces are updated accordingly. The calculation of the state-dependent forces is treated in more detail in Section 3.3.

3.1. Mathematical model of the track

The complex modal superposition technique adopted here was developed elsewhere, see Abrahamsson [14]. The technique has previously been used with linear track models as presented by Nielsen et al. [5,6]. Here the approach to use complex modal superposition in the presence of state-dependent track properties is advanced.

The coupled second order equations of motion of the state-dependent track model with N degrees-of-freedom can be written in first order state–space form as

$$\mathbf{A}^{track}\dot{\mathbf{y}}^{track}(t)+\mathbf{B}^{track}\mathbf{y}^{track}(t)=\left\{\begin{array}{c}\mathbf{F}^{track}(t)\\ \mathbf{0}\end{array}\right\}, \tag{2}$$

$$\mathbf{y}^{track}(t)=\left\{\begin{array}{c}\mathbf{x}^{track}(t)\\ \dot{\mathbf{x}}^{track}(t)\end{array}\right\}, \tag{3}$$

$$\mathbf{A}^{track}=\left[\begin{array}{cc}\mathbf{C}^{track} & \mathbf{M}^{track}\\ \mathbf{M}^{track} & \mathbf{0}\end{array}\right], \tag{4}$$

and

$$\mathbf{B}^{track}=\left[\begin{array}{cc}\mathbf{K}^{track} & \mathbf{0}\\ \mathbf{0} & -\mathbf{M}^{track}\end{array}\right]. \tag{5}$$

Here $\mathbf{A}^{track}$ and $\mathbf{B}^{track}$ are $2N\times 2N$ matrices which contain the linear contributions of the state-dependent track properties. The state–space vector $\mathbf{y}^{track}$ includes the nodal displacements $\mathbf{x}^{track}$ and nodal velocities $\dot{\mathbf{x}}^{track}$ of the track model. The external load vector $\mathbf{F}^{track}$ includes contributions both from wheel–rail contact forces $\mathbf{F}^{w/r}$ and forces $\mathbf{F}^{sd}$ accounting for the state-dependent track property increments.

Since the homogeneous problem corresponding to Eqs. (2)–(5) is linear and self-adjoint, its complete modal solution can be determined from the standard linear algebraic eigenvalue problem, see for example Ref. [15] (complex quantities are indicated by an underbar):

$$\left[\begin{array}{cc}\mathbf{K}^{track^{-1}}\mathbf{C}^{track} & \mathbf{K}^{track^{-1}}\mathbf{M}^{track}\\ -\mathbf{I} & \mathbf{0}\end{array}\right]\left\{\begin{array}{c}\underline{\boldsymbol{\rho}}^{(n)}\\ \mathrm{i}\underline{\omega}_n\underline{\boldsymbol{\rho}}^{(n)}\end{array}\right\}=-\frac{1}{\mathrm{i}\underline{\omega}_n}\left\{\begin{array}{c}\underline{\boldsymbol{\rho}}^{(n)}\\ \mathrm{i}\underline{\omega}_n\underline{\boldsymbol{\rho}}^{(n)}\end{array}\right\}. \tag{6}$$

Provided that the damping is low, the solution to the eigenvalue problem in Eq. (6) yields N pairs of complex-conjugated sets of eigenvalues $\mathrm{i}\underline{\omega}_n$ and eigenvectors $\underline{\boldsymbol{\rho}}^{(n)}$. The eigenvectors are assembled in the modal matrix

$$\underline{\mathbf{P}}=\left[\begin{array}{ccc}\underline{\boldsymbol{\rho}}^{(1)} & \cdots & \underline{\boldsymbol{\rho}}^{(2N)}\\ \mathrm{i}\underline{\omega}_1\underline{\boldsymbol{\rho}}^{(1)} & \cdots & \mathrm{i}\underline{\omega}_{2N}\underline{\boldsymbol{\rho}}^{(2N)}\end{array}\right]. \tag{7}$$

The equations of motion in Eqs. (2)–(5) are transformed into modal space by using the transformations

$$\mathbf{y}^{track}(t)=\underline{\mathbf{P}}\underline{\mathbf{q}}^{track}(t) \tag{8}$$

and

$$\underline{\mathbf{Q}}^{track}(t)=\underline{\mathbf{P}}^{\mathrm{T}}\left\{\begin{array}{c}\mathbf{F}^{track}(t)\\ \mathbf{0}\end{array}\right\} \tag{9}$$

with T denoting the transpose of a matrix. Here $\underline{\mathbf{q}}^{track}(t)$ is the modal displacement vector with elements $\underline{q}_n^{track}(t)$, and $\underline{\mathbf{Q}}^{track}(t)$ is the modal load vector with elements $\underline{Q}_n^{track}(t)$. The modal load

vector contains contributions $\underline{\mathbf{Q}}^{w/r}(t)$ from the wheel–rail contact forces and $\underline{\mathbf{Q}}^{sd}(t)$ from the state-dependent track property increments. Due to the orthogonality properties of the modal matrix, a full decoupling of the equations of motion for the track model with a non-proportional spatial distribution of viscous damping is obtained. The $2N$ uncoupled equations of motion determining the response from the transient loading of the track are obtained as in Ref. [16] ($n = 1, 2, \ldots, 2N$):

$$diag(\underline{a}_n)\dot{\underline{\mathbf{q}}}^{track}(t) + diag(\underline{b}_n)\underline{\mathbf{q}}^{track}(t) = \underline{\mathbf{Q}}^{track}(t) \tag{10}$$

with the modal normalization constants

$$diag(\underline{a}_n) = \underline{\mathbf{P}}^{\mathrm{T}}\mathbf{A}^{track}\underline{\mathbf{P}} \tag{11a}$$

and

$$diag(\underline{b}_n) = \underline{\mathbf{P}}^{\mathrm{T}}\mathbf{B}^{track}\underline{\mathbf{P}}. \tag{11b}$$

The modal stiffness $\underline{b}_n$ and the modal damping $\underline{a}_n$ are related to the nth eigenvalue $\mathrm{i}\underline{\omega}_n$ as

$$-\mathrm{i}\underline{\omega}_n\underline{a}_n = \underline{b}_n. \tag{12}$$

In the modal synthesis, the mode set is normally truncated to achieve a better computational efficiency (see Ref. [17]). This approach is acceptable when the high-frequency components of the exciting forces are negligible. In such a case, the excitation of the truncated high-frequency modes and their contributions to dynamic responses will be small. However, the quasi-static contribution from the truncated modes may not always be negligible. This is for example the case when displacements and sectional forces are calculated in a structure (see Ref. [18]). In the present study, the quasi-static contributions will be accounted for when rail pad deformations, sleeper displacements and rail bending moments are calculated. An attractive approach to account for the quasi-static contribution of the truncated modes without analyzing these modes individually is described by Abrahamsson and Lundblad [16] and Clough and Penzien [18].

The contributions Δe_{jk} from the truncated high-frequency modes to the elements of the flexibility matrix are calculated as

$$\Delta e_{jk} = \underline{e}_{jk}(\omega_{ref}) - \sum_{n=1}^{2M} \frac{\underline{\rho}_j^{(n)}\underline{\rho}_k^{(n)}}{\mathrm{i}\underline{a}_n(\omega_{ref} - \underline{\omega}_n)}, \tag{13}$$

where M is the number of retained complex-conjugated modal pairs. The dynamic flexibility matrix $\underline{\mathbf{e}}$ is evaluated at a frequency ω_{ref} which is much lower than any of the eigenfrequencies of the truncated modes. In the example in this study, $\omega_{ref} = 0$. The quasi-static contribution $\Delta\mathbf{x}^{qs}$ to the calculated dynamic displacement in Eq. (8) is obtained as

$$\Delta\mathbf{x}^{qs}(t) = \Delta\mathbf{e}\mathbf{F}^{track}(t). \tag{14}$$

3.2. Solution of the interaction problem

A general approach to simulate train–track interaction in the time domain was advanced in Nielsen and Abrahamsson [5]. A mixed extended state–space vector was introduced,

$$\underline{\mathbf{z}}(t) = \left\{ \underline{\mathbf{q}}^{track\mathrm{T}} \quad \mathbf{x}^{train\mathrm{T}} \quad \dot{\mathbf{x}}^{train\mathrm{T}} \quad \hat{\mathbf{F}}^{w/r\mathrm{T}} \right\}^{\mathrm{T}}. \tag{15}$$

This vector is mixed in the sense that it contains modal displacements $\underline{\mathbf{q}}^{track}$ of the track, physical displacements $\mathbf{x}^{train}$ and velocities $\dot{\mathbf{x}}^{train}$ of the train, and impulses $\hat{\mathbf{F}}^{w/r} = \int \mathbf{F}^{w/r}(t)\,\mathrm{d}t$ of wheel–rail contact forces. In its general form, the system of time-variant equations for the coupled train–track system is assembled in first order matrix form as [5,6]

$$\underline{\mathbf{A}}(\underline{\mathbf{z}}, t)\dot{\underline{\mathbf{z}}} + \underline{\mathbf{B}}(\underline{\mathbf{z}}, t)\underline{\mathbf{z}} = \underline{\mathbf{F}}(\underline{\mathbf{z}}, t). \tag{16}$$

The equation system (16) contains the governing equations of motion for train and track together with the algebraic constraint equations that are used to couple the train to the track. The given (time-variant) train speed is entered into the model through the constraint equations, and the Coriolis and centripetal accelerations that occur because the train model is moving along the track model are accounted for. The contents of the two matrices are described in detail in Ref. [6]. Since the addition of state-dependent track properties will have no influence on $\underline{\mathbf{A}}$ and $\underline{\mathbf{B}}$, these matrices are not repeated here. Note that the contribution $\underline{\mathbf{Q}}^{w/r}$ to the total modal load $\underline{\mathbf{Q}}^{track}$ is accounted for within the product $\underline{\mathbf{A}}\dot{\underline{\mathbf{z}}}$. The mixed force vector $\underline{\mathbf{F}}$ is written as

$$\underline{\mathbf{F}}(\underline{\mathbf{z}}, t) = \left\{ \underline{\mathbf{Q}}^{sd\mathrm{T}}(t) \quad \mathbf{F}^{train\mathrm{T}}(t) \quad -\ddot{\mathbf{x}}^{irr\mathrm{T}}(t) \quad -\dot{\mathbf{x}}^{irr\mathrm{T}}(t) \right\}^{\mathrm{T}}. \tag{17}$$

Here $\mathbf{F}^{train}$ is a vector containing given external loads acting on the train (such as axle loads), and $\mathbf{x}^{irr}$ is a vector containing information about the surface irregularities on wheel treads and railhead leading to a prescribed relative wheel–rail displacement excitation. The new component in $\underline{\mathbf{F}}$ is the state-dependent modal load vector $\underline{\mathbf{Q}}^{sd}$. The calculation of $\underline{\mathbf{Q}}^{sd}$ is discussed in Section 3.3. An initial value problem for the solution of the transient vibration problem is obtained as

$$\dot{\underline{\mathbf{z}}} = \underline{\mathbf{A}}^{-1}(\underline{\mathbf{F}} - \underline{\mathbf{B}}\underline{\mathbf{z}}), \quad \underline{\mathbf{z}}(t = 0) = \underline{\mathbf{z}}_0, \tag{18}$$

where $\underline{\mathbf{z}}_0$ is the initial state. The first order format allows for a rational numerical solution by use of any of several existing time-integration methods. In the present study, solutions are obtained using MATLAB's stiff differential equation solver ode15s.

3.3. State-dependent modal loads

The external force $\mathbf{F}^{sd}(t)$ (a partition of the load vector $\mathbf{F}^{track}(t)$ in Eq. (2)) accounting for the state-dependent increments of the track properties contains contributions from rail pads and ballast/subgrade as

$$\mathbf{F}^{sd}(t) = \mathbf{F}^{pad}(t) + \mathbf{F}^{b/s}(t). \tag{19}$$

The separation of state-dependent track properties in linear contributions and time-variant increments is schematically illustrated in Fig. 5. Let $f_i^{pad}(\underline{\mathbf{z}}, t)$ and $g_i^{pad}(\underline{\mathbf{z}}, t)$ be general expressions describing the state-dependent load–displacement and load–velocity characteristics of the ith rail pad. Then the state-dependent contribution to the total force acting on this rail pad is

$$F_i^{pad}(\underline{\mathbf{z}}, t) = f_i^{pad}(\underline{\mathbf{z}}, t) - k_{pi}^{lin}\Delta x_i^{pad}(t) + g_i^{pad}(\underline{\mathbf{z}}, t) - c_{pi}^{lin}\Delta \dot{x}_i^{pad}(t), \tag{20}$$

where k_{pi}^{lin} and c_{pi}^{lin} are the linear contributions to the stiffness and damping properties of rail pad i which are already accounted for in the matrices $\mathbf{K}^{track}$ and $\mathbf{C}^{track}$. The physical deformation Δx_i^{pad} and deformation rate $\Delta \dot{x}_i^{pad}$ of rail pad i are calculated from a modal sum with the $2M$ retained

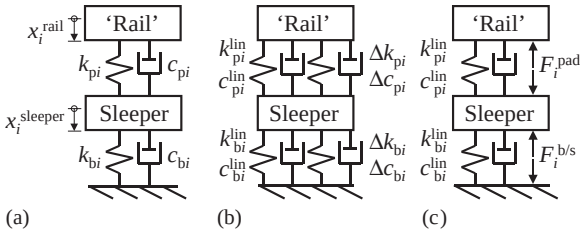

Fig. 5. Principal illustration of how (a) state-dependent stiffnesses and dampings of rail pads and ballast/subgrade are (b) separated in linear contributions (k_{pi}^{lin}, c_{pi}^{lin}, k_{bi}^{lin} and c_{bi}^{lin}) and time-variant increments (Δk_{pi}, Δc_{pi}, Δk_{bi} and Δc_{bi}). In the simulation, the time-variant increments of stiffness and damping associated with the time-dependent position of the vehicle load are accounted for by (c) applying equivalent external forces, F_i^{pad} and $F_i^{b/s}$, to the corresponding nodes of rail and sleepers. Index i is used to distinguish between different sleepers.

modes, cf., Eq. (8),

$$\Delta x_i^{pad} = x_i^{rail} - x_i^{sleeper} = \sum_{n=1}^{2M} (\underline{\rho}_i^{rail})^{(n)} \underline{q}_n^{track} - \sum_{n=1}^{2M} (\underline{\rho}_i^{sleeper})^{(n)} \underline{q}_n^{track} \tag{21}$$

and

$$\Delta \dot{x}_i^{pad} = \dot{x}_i^{rail} - \dot{x}_i^{sleeper} = \sum_{n=1}^{2M} \mathrm{i}\underline{\omega}_n (\underline{\rho}_i^{rail})^{(n)} \underline{q}_n^{track} - \sum_{n=1}^{2M} \mathrm{i}\underline{\omega}_n (\underline{\rho}_i^{sleeper})^{(n)} \underline{q}_n^{track}. \tag{22}$$

The quasi-static contributions from the truncated modes $n > 2M$ to the dynamic displacements in Eq. (21) are calculated according to Eq. (14). The elements $(\underline{\rho}_i^{rail})^{(n)}$ and $(\underline{\rho}_i^{sleeper})^{(n)}$ of the modal matrix correspond to the physical displacements and velocities of the degrees of freedom (d.o.f.'s) on rail and sleeper that are coupled to rail pad i.

The contribution from rail pad i to the total modal load is obtained as

$$(\underline{Q}_i^{pad})_n = \left\{ (\underline{\rho}_i^{sleeper})^{(n)} - (\underline{\rho}_i^{rail})^{(n)} \right\} F_i^{pad}, \tag{23}$$

where the sign convention assumes that physical displacements of rail and sleepers are both positive downwards. A similar procedure can be adopted to derive contributions from the ballast/subgrade when the sleepers are modelled as rigid with only one d.o.f. The state-dependent contribution from the ballast/subgrade to the total force acting on sleeper i is obtained as

$$F_i^{b/s}(\underline{\mathbf{z}}, t) = f_i^{b/s}(\underline{\mathbf{z}}, t) - k_{bi}^{lin} x_i^{sleeper}(t) + g_i^{b/s}(\underline{\mathbf{z}}, t) - c_{bi}^{lin} \dot{x}_i^{sleeper}(t). \tag{24}$$

The contribution from the ballast/subgrade under sleeper i to the total modal load is calculated as

$$(\underline{Q}_i^{b/s})_n = -(\underline{\rho}_i^{\mathrm{sleeper}})^{(n)} F_i^{b/s}. \tag{25}$$

The total modal load $\underline{\mathbf{Q}}^{sd}$ is obtained by adding contributions from all rail pads and ballast/subgrade components in the track model. To save computing time, the six rail pads and six ballast/subgrade components nearest to each wheel load have been accounted for in the demonstration example below. The contribution from the other components is negligible.

Note that the state-dependent modal loads can be extended to account for other states than only the displacement and velocity of rail pads and ballast/subgrade suggested here. For example,

if the pertinent data are available, a state-dependent inertia of the ballast/subgrade due to the moving wheel loads can be included by adding an acceleration term to Eq. (24).

4. Demonstration example

Linear stiffnesses and viscous dampings of rail pads and ballast/subgrade have been determined by tuning the calculated vertical direct receptance (amplitude and phase of displacement over applied force versus excitation frequency) of the rail to the corresponding receptance measured at the test site. The receptance was measured for the track without static preload by exciting the rail at the centre of a sleeper bay with a sledgehammer. The agreement between measured and calculated receptances is illustrated in Fig. 6. Tuned track properties are listed in Table 1. It is observed in Table 1 that the tuned linear ballast stiffness 30 MN/m fits well within the range of secant stiffnesses in Fig. 1 when these are extrapolated to an unloaded track (zero sleeper force).

The first resonance frequency in Fig. 6 is obtained at around 60 Hz. At this resonance, rail and sleepers are vibrating in phase on the ballast. A second resonance, with a large relative motion of rail and sleepers, is obtained at approximately 250 Hz. This resonance frequency is to a large extent determined by rail pad properties. The sharp peak above 900 Hz is the pinned–pinned rail resonance. At this resonance, the rail vibrates with a wavelength equal to two sleeper bays with nodes above the sleepers, and with a slow decay of vibration amplitude along its length. The boundaries of the finite track model lead to wave reflections, and thus the observed irregularities in the calculated receptance around this resonance. However, the influence of these irregularities on the calculated response considered in the present demonstration example is negligible.

Using the results in Figs. 1, 2 and 6, a state-dependent ballast/subgrade model (representing the test site on Svealandsbanan) has been derived. Unfortunately, measured data from unfastened sleepers are only available for the excitation frequency 2 Hz. For the assembled track, the direct receptance was measured in the frequency range 10–2000 Hz, but in this case in the absence of a

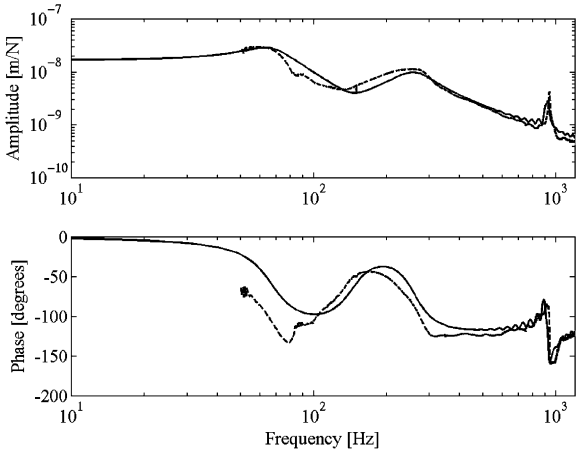

Fig. 6. Amplitude and phase of measured (- - - -) and calculated (——) direct track receptance of rail at midspan. Track without static preload (Svealandsbanan, 2000).

static preload. Due to the limited amount of information, some assumptions in the modelling of the ballast/subgrade must be made. For example, it is assumed here that all sleepers in the track model are supported by the linear ballast/subgrade stiffness 30 MN/m. Further, based on the information in Fig. 1, it is assumed that for the sleepers near a wheel load, the ballast/subgrade secant stiffness increases proportionally with sleeper load according to

$$k_{secant}^{b/s} = 2 \times 10^3 F_i^{b/s} + 30 \times 10^6 \quad (\mathrm{N/m}). \tag{26}$$

For different given sleeper loads $F_i^{b/s}$, the corresponding sleeper displacements have been calculated; see the square markers in Fig. 7. A fourth-degree polynomial was adopted to mimic the measured ballast/subgrade load–displacement characteristic. The component $(F_i^{b/s})_k$ of the force on sleeper i due to the state-dependent stiffness of the ballast/subgrade is given here as (note that the linear term omitted in Eq. (27) is already accounted for in the modal model of the track)

$$(F_i^{b/s})_k(\underline{\mathbf{z}}, t) = \begin{cases} \alpha(x_i^{sleeper}(t))^2 + \beta(x_i^{sleeper}(t))^3 + \delta(x_i^{sleeper}(t))^4 & \text{if } x_i^{sleeper} > 0, \\ 0 & \text{else} \end{cases} \tag{27}$$

with $\alpha = 0.37 \times 10^{12}\,\mathrm{N/m^2}$, $\beta = -2.47 \times 10^{15}\,\mathrm{N/m^3}$ and $\delta = 5.75 \times 10^{18}\,\mathrm{N/m^4}$.

The structural damping of the ballast/subgrade needs to be translated into viscous damping before it can be used in the train–track interaction time-integration algorithm. The lowest track resonance at 60 Hz in Fig. 6 is to a large extent determined by the linear ballast/subgrade properties listed in Table 1. At this frequency, an equivalent structural damping is given by

$$\eta = \frac{\omega c_b^{lin}}{k_b^{lin}} = \frac{2\pi \times 60 \times 31 \times 10^3}{30 \times 10^6} = 0.39. \tag{28}$$

This loss factor is in the same order of magnitude as the loss factors reported in Fig. 2. Since the loss factor seems to be relatively independent of sleeper load, a state-dependent ballast/subgrade

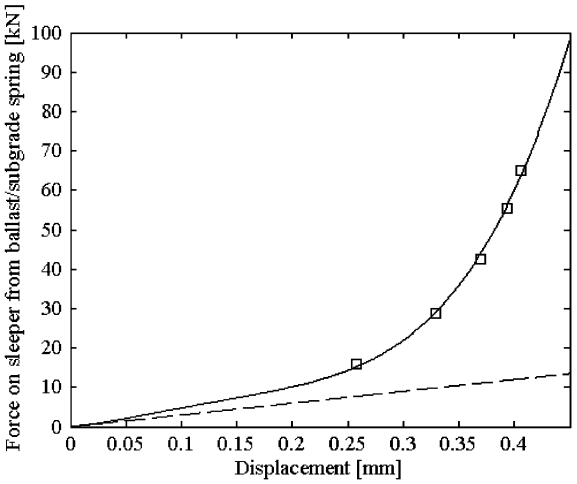

Fig. 7. Load–displacement characteristics for (1) a state-dependent ballast/subgrade model (——) based on measured data (□) and (2) a linear ballast/subgrade model (- - - -).

viscous damping model leading to the loss factor 0.39 at 60 Hz independent of sleeper load has been selected. This is achieved if the quotient

$$\tau = \frac{c_b^{sd}}{k_b^{sd}} = \frac{c_b^{lin}}{k_b^{lin}} \tag{29}$$

is constant. Then it can be shown that the state-dependent viscous force on sleeper i is determined by

$$(F_i^{b/s})_c(\underline{\mathbf{z}}, t) = \begin{cases} \tau \dot{x}_i^{sleeper} \left[\alpha(x_i^{sleeper}(t)) + \beta(x_i^{sleeper}(t))^2 + \delta(x_i^{sleeper}(t))^3 \right] & \text{if } x_i^{sleeper} > 0, \\ 0 & \text{else.} \end{cases} \tag{30}$$

The total state-dependent load on each sleeper is determined by adding the contributions in Eqs. (27) and (30). One bogie in the train is modelled by two rigid moving masses. Each moving mass corresponds to half the unsprung mass of one wheelset (only half the bogie is modelled because the track and its loading are assumed to be symmetric). In the frequency range of interest in the present study, the dynamics of car body and bogie frames are decoupled from the wheelsets by the soft primary and secondary bogie suspensions. Thus, a static load representing half the axle load is acting on each unsprung mass. A non-linear compressive stiffness of each wheel–rail contact is determined by assuming three-dimensional contact mechanics according to Hertz. The Hertzian contact stiffness coefficient $C_H = 9.17 \times 10^{10}\ \mathrm{N/m^{3/2}}$ is determined by taking the curve radii 0.45 m and ∞ for the wheel, and ∞ and 0.30 m for the rail. This corresponds to a wheel with diameter 900 mm and a conical transverse profile rolling on a straight rail with a curved railhead.

During the extensive field measurement campaign on Svealandsbanan in 2000, the influence of different types of wheel out-of-roundness on dynamic wheel–rail contact force and track response was also investigated. A freight train with six four-axle wagons was equipped with wheelsets having different types of defect including wheel flats, polygonal wheels and spalls from surface or subsurface initiated rolling contact fatigue. Wheel–rail contact forces were measured using a wheel impact load detector with strain gauges on the rail web in nine consecutive sleeper bays. Strain gauges were also positioned on the railfoot at 11 locations along the track at midspan and above sleepers. In total, 40 track responses were recorded simultaneously at each train passage with a sampling frequency of 6 kHz. The test site and the instrumented track are depicted in Fig. 8. Train speeds were varied between 5 and 100 km/h. Each load case with a specified combination of axle load and train speed was run three times. The test campaign is described in more detail in Ref. [19].

Wheel–rail contact forces and rail bending moments have been simulated by using the mathematical model described in Section 3. The investigated wheel out-of-roundness is a 100 mm long and 0.9 mm deep wheel flat. The measured profile on a single line along the wheel flat was used as excitation input. By synchronizing measured and calculated responses, it was concluded that the centre of the wheel flat came in contact with the rail approximately 25 mm after the centre of one instrumented sleeper bay, and that this position did not vary much between different load cases. The time history of the contact force caused by a wheel flat has a characteristic shape: The response begins with a sudden drop due to the increasing radial deviation from the nominal wheel radius. During this phase, the wheel will move downwards and the rail upwards to compensate for the missing wheel material. In several cases, there is a loss of wheel–rail contact. After passing the

Fig. 8. Test site on Svealandsbanan (2000): (a) Photograph of the track; (b) instrumentation on rail and sleepers, including strain gauges on the rail web, on the railfoot and on the sleepers and accelerometers underneath the railhead and on top of the sleepers.

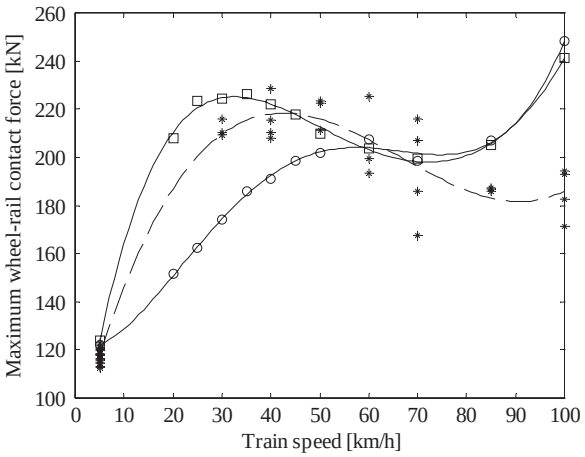

Fig. 9. Peak wheel–rail contact force versus train speed for a 100 mm long and 0.9 mm deep wheel flat. Measured data: ∗, state-dependent track model; □, linear track model: ○, Svealandsbanan, 2000.

centre of the wheel flat where the radial deviation starts to decrease back towards the nominal radius, the wheel will continue downwards due to its greater inertia forcing the rail to do the same. This results in a peak force. Calculated peak forces and peak rail bending moments using the state-dependent track model presented here are shown as square markers in Figs. 9 and 10. Measured peak values for different train passages are marked by asterisks. In order to illustrate the influence of train speed, fifth order polynomials have been fitted to the measured and calculated responses.

A local maximum in the measured peak wheel–rail contact force seems to be obtained at 40 km/h. Simulation with the state-dependent track model using a higher train speed resolution than was available from the test campaign predicts a contact force maximum at 35 km/h. The train–track interaction algorithm with the state-dependent track model predicts measured

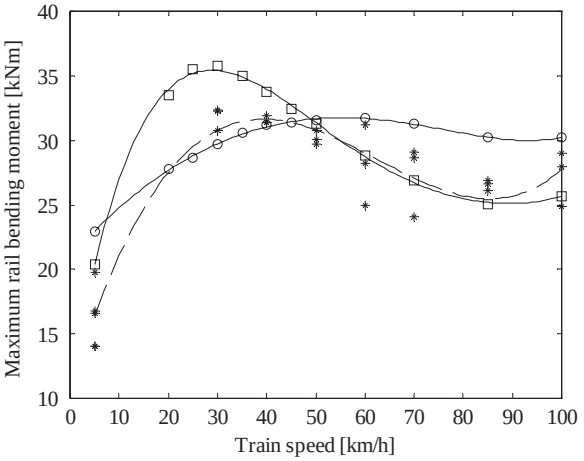

Fig. 10. Peak rail bending moment versus train speed for a 100 mm long and 0.9 mm deep wheel flat. Measured data: ∗, state-dependent track model; □, linear track model; ○, Svealandsbanan, 2000.

responses with the (under these circumstances) high level of accuracy of roughly 10%. Calculated results obtained when the state-dependence is neglected are shown as circles in Figs. 9 and 10. It is observed that accounting for state-dependent track properties improves the agreement with measured data. For train speed 40 km/h, the state-dependent track model predicts a maximum sleeper displacement 0.45 mm in the presence of the studied wheel flat (0.39 mm without the wheel flat). Referring to the non-linear load–displacement characteristics of the ballast/subgrade illustrated in Fig. 7, it is concluded that with such a range of sleeper displacements (0–0.45 mm), the use of a state-dependent track model instead of a linear track model is clearly indicated.

5. Concluding remarks

The state-dependence of railway track components such as rail pads and ballast/subgrade has been discussed with reference to field and laboratory measurements. It has been demonstrated that both rail pads and ballast/subgrade exhibit load–displacement characteristics that are strongly non-linear and dependent on the static (or low-frequency) load magnitude. Most train–track interaction models available in the literature are either fully linear (frequency-domain models) or linear except for the conditions at the wheel–rail contact (time-domain models). Depending on the type of investigated response, the influence of the state-dependent properties of rail pads and ballast/subgrade may be quite significant. For example, rail and sleeper bending moments will be dependent on a correct description of the stiffness of rail pads and ballast/subgrade. A numerical approach to account for such state-dependent properties in a previously developed method for simulation of dynamic train–track interaction has therefore been proposed. Track properties are separated into linear contributions corresponding to an unloaded track and non-linear contributions that are dependent on the time-variant state of the different track components due to the dynamic loading from a moving train model. In the present study, the state-dependent contributions to the modal loads are determined by the displacement and velocity

states of rail pads and ballast/subgrade (see Eqs. (20) and (24)). However, the modal loads can just as well be expressed in a more general form if such information is available.

The numerical method and the state-dependent track model have been validated versus field measurements of wheel–rail contact force and rail bending moment caused by a 100 mm long and 0.9 mm deep wheel flat. The good agreement between calculated and measured responses encourages future use of the state-dependent track model.

Acknowledgements

The theoretical part of this work, which was presented in Section 3, was performed during the Brite/EuRam III project "Silent Track" and documented in a Ph.D. thesis [20]. The work was performed within the Centre of Excellence CHARMEC (CHAlmers Railway MEChanics) at Chalmers University of Technology. Field tests were planned in co-operation with the Swedish National Rail Administration (Banverket) and staff at the Department of Applied Mechanics, Chalmers University of Technology. Mr. Eric Berggren and Mr. Jan Gomersson from Banverket performed the field tests. Discussions with Professor Thomas Abrahamsson and Professor Bengt Åkesson are gratefully acknowledged.

References

[1] K. Knothe, S.L. Grassie, Modelling of railway track and vehicle/track interaction at high frequencies, *Vehicle System Dynamics* 22 (3–4) (1993) 209–262.

[2] K. Popp, H. Kruse, I. Kaiser, Vehicle–track dynamics in the mid-frequency range, *Vehicle System Dynamics* 31 (5–6) (1999) 423–464.

[3] D.J. Thompson, Wheel–rail noise generation, parts I–V, *Journal of Sound and Vibration* 161 (3) (1993) 387–482.

[4] K. Hempelmann, *Short-pitch Corrugation on Railway Rails—A Linear Model for Prediction*, Reihe 12 (213), VDI Fortschritt-Berichte, Düsseldorf, 1994.

[5] J.C.O. Nielsen, T.J.S. Abrahamsson, Coupling of physical and modal components for analysis of moving non-linear dynamic systems on general beam structures, *International Journal for Numerical Methods in Engineering* 33 (9) (1992) 1843–1859.

[6] J.C.O. Nielsen, A. Igeland, Vertical dynamic interaction between train and track—influence of wheel and track imperfections, *Journal of Sound and Vibration* 187 (5) (1995) 825–839.

[7] B. Ripke, *Hochfrequente Gleismodellierung und Simulation der Fahrzeug-Gleis-Dynamik unter Verwendung einer nichtlinearen Kontaktmechanik*, Reihe 12 (249), VDI Fortschritt-Berichte, Düsseldorf, 1995.

[8] M. Fermér, J.C.O. Nielsen, Vertical interaction between train and track with soft and stiff rail pads—full-scale experiments and theory, *Proceedings of the Institution of Mechanical Engineers. Part F—Journal of Rail and Rapid Transit.* 209 (1995) 39–47.

[9] A. Igeland, J. Oscarsson, Modelling of railway track for computer simulation of dynamic train-track interaction, *Proceedings of the 15th International Modal Analysis Conference*, Tokyo, Japan, 1997, pp. 464–470.

[10] B.J. Lazan, *Damping of Materials and Members in Structural Mechanics*, 1st Edition, Pergamon, Oxford, 1968, 317pp.

[11] D.J. Thompson, W.J. van Vliet, Measurements of the high-frequency dynamic properties of Swedish rail pads, Report TPD-HAG-RPT-960066, TNO Institute of Applied Physics, Delft, the Netherlands, 1996.

[12] D.J. Thompson, C.J.C. Jones, T.X. Wu, G. de France, The influence of the non-linear stiffness behaviour of rail pads on the track component of rolling noise, *Proceedings of the Institution of Mechanical Engineers. Part F—Journal of Rail and Rapid Transit* 213 (1999) 233–241.

[13] C. Andersson, J. Oscarsson, Dynamic train/track interaction including state-dependent track properties and flexible vehicle components, *Vehicle System Dynamics Supplement* 33 (1999) 47–58.
[14] T.J.S. Abrahamsson, Modal Analysis and Synthesis in Transient Vibration and Structural Optimization Problems, Ph.D. Dissertation, Department of Solid Mechanics, Chalmers University of Technology, Göteborg, Sweden, 1990.
[15] L. Meirovitch, *Principles and Techniques of Vibrations*, Prentice-Hall, London, 1997.
[16] T.J.S. Abrahamsson, M. Lundblad, Göteborg, Sweden, Transient vibration analysis of non-proportionally damped linear structures using modal parameters, Technical Report F105, Department of Solid Mechanics, Chalmers University of Technology, 1987.
[17] D.J. Ewins, *Modal Testing Theory and Practice*, Wiley, New York, 1984.
[18] R.W. Clough, J. Penzien, *Dynamics of Structures*, 2nd Edition, McGraw-Hill, New York, 1993.
[19] A. Johansson, J.C.O. Nielsen, Out-of-round railway wheels—wheel-rail contact forces and track response from full-scale measurements and numerical simulations, *Proceedings of the Institution of Mechanical Engineers. Part F—Journal of Rail and Rapid Transit* 217 (2003) 135–146.
[20] J. Oscarsson, Dynamic Train–track Interaction: Linear and Non-linear Track Models with Property Scatter, Ph.D. Thesis, Department of Solid Mechanics, Chalmers University of Technology, Göteborg, Sweden, 2001.